Artificial Life and Robotics (2024) 29:349–357
https://doi.org/10.1007/s10015-024-00943-w

ORIGINAL ARTICLE

Development of a rimless wheel robot with telescopic legs for step adaptability

Yuta Hanazawa[1] · **Yuhi Uchino**[1] · **Shinichi Sagara**[1]

Received: 12 October 2023 / Accepted: 8 February 2024 / Published online: 26 March 2024

Abstract
In this study, we developed a rimless wheel robot with elastic telescopic legs that can overcome steps. Numerical studies have shown that a rimless wheel robot with elastic telescopic legs has high adaptability to steps. However, rimless wheel robots that can walk in environments with steps have not yet been developed. To develop a rimless wheel robot that could overcome the steps, we initially developed a three-dimensional model of the robot through Unity software and simulated its walking on level ground and surfaces with steps. Then, we determined the optimal elasticity of the elastic telescopic legs through numerical simulation and constructed a model with optimized parameters. Finally, we conducted the walking experiments employing the developed robot. The robot can walk on level ground and surfaces with steps.

Keywords Walking robot · Rimless wheel · Telescopic leg

1 Introduction

Recently, mobile robots with special leg mechanisms have been developed [1, 2]. We have studied mobile robots with rimless wheels. A rimless wheel has only a hub and spokes without a rim [3, 4]. Instead of rolling movement, a wheel essentially undergoes a walking motion without a rim. Therefore, such a wheel can travel uneven terrain similar to a general walking robot, and this, particularly, gives researchers an interest in its ability to overcome the steps.

Robots with the wheels are called "rimless wheel robots" and have been studied [5–8]. Moreover, rimless wheel robots with elastic telescopic legs have been proposed. Based on the numerical simulation results, Asano et al. presented that rimless wheel robots have a high adaptability to steps due to the elasticity of the telescopic legs [9–11].

✉ Yuta Hanazawa
hanazawa@cntl.kyutech.ac.jp

Yuhi Uchino
uchino.yuhi970@mail.kyutech.jp

Shinichi Sagara
sagara@cntl.kyutech.ac.jp

[1] Department of Mechanical and Control Engineering, Kyushu Institute of Technology, 1-1 Sensui, Tobata, Kitakyushu, Fukuoka 804-8550, Japan

However, experimental studies are required on the rolling motion of rimless wheels with elastic telescopic legs to confirm their adaptability. Similar robotics research has developed a robot that can climb high steps with actively moving telescopic legs [12]. Furthermore, we want to realize a robot that can move fast and passively handle steps. This means moving at high speed on a stepped surface in a concrete real-life situation. Figure 1 shows a schematic of the rimless wheel robot. The robot has a torso and legs that can stretch and contract due to the elastic spring.

However, no developments on rimless wheel robots that can walk on level ground with steps. Altough rimless wheel robots with elastic telescopic legs is being developed, the elasticity of their legs aims shock absorption rather than traversing steps [13, 14]. To better understand the performance of such robots, it is required to investigate their behavior while climbing up and down steps through walking experiments with actual robots.

It is necessary to determine the parameters of the robot to develop an experimental machine, particularly the elasticity of the telescopic leg with a substantial effect on gait. Additionally, although simple two-dimensional (2D) walking simulations were reported, there is still a need for gait analysis using three-dimensional (3D) walking simulations, which were closely simulated in real environments.

In this study, we first developed a robot model and simulated its walking on level ground and surfaces with steps,

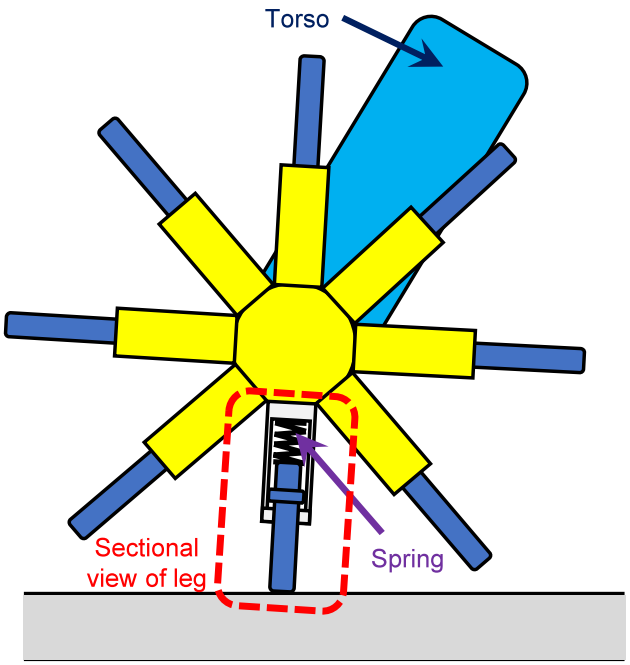

Fig. 1 Schematic illustrating a rimless wheel robot with elastic telescopic legs

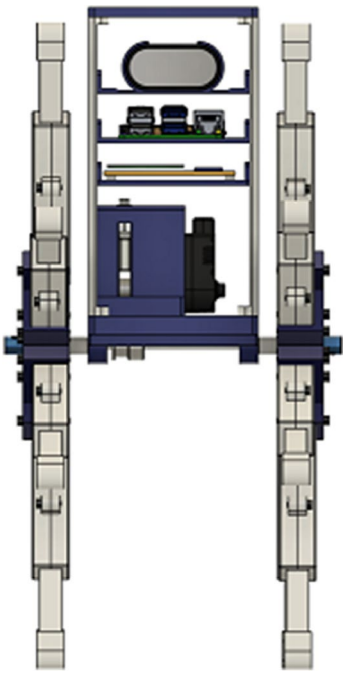

Fig. 3 Frontal perspective of 3D model of the rimless wheel robot

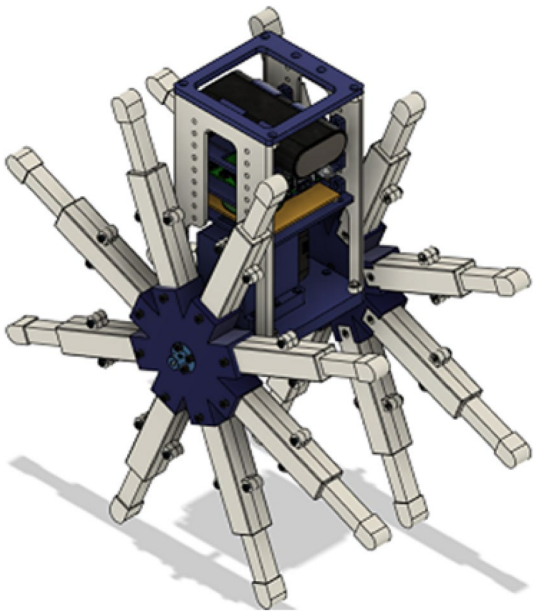

Fig. 2 3D model representation of the rimless wheel robot with elastic telescopic legs: an overview

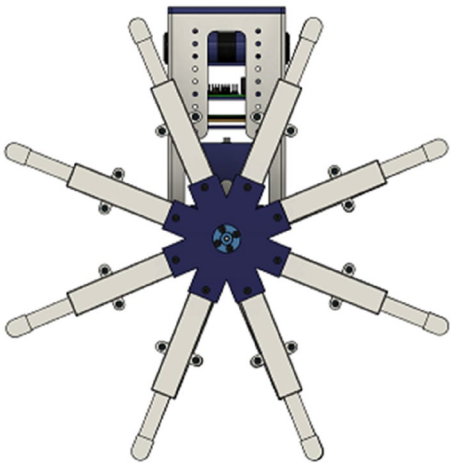

Fig. 4 Lateral perspective of 3D model of the rimless wheel robot

and built the actual robot. Figures 2, 3 and 4 demonstrate the 3D model of the rimless wheel robot built using 3D computer-aided design (CAD) software. The 3D walking of a rimless wheel robot with telescopic legs shows very complex dynamics and it is unrealistic to create such a model after deriving all the equations of motion and impact equations as in previous studies. Thus, we simulated the walking of the robot in Unity [15]. We obtained the optimum elasticity of the legs suitable to overcoming steps. Based on the simulation results, we constructed a rimless wheel robot with elastic legs, optimized for overcoming steps. Finally, we conducted walking experiments using a rimless wheel robot with the optimum elasticity to overcome steps. The rest of this paper is organized as follows. Section 2 introduces the model of the rimless wheel robot in Unity. Section 3 presents the output-zeroing control method. Section 4 displays the numerical simulation results of the walking simulator.

Section 5 highlights the constructed rimless wheel robot and the experimental results. Finally, Sect. 6 presents the conclusion and discusses future directions.

2 Model of the rimless wheel robot in unity

In this section, we detail of the rimless wheel robot model with elastic telescopic legs developed in Unity. We constructed a 3D model of the robot (Fig. 5) which is less complex than the 3D model of the actual robot (Fig. 2). The parameters were determined using 3D CAD software.

Initially, we equipped the robot's tiptoe with a sphere collider to detect collisions. However, we observed certain phenomena, such as skidding. To address this, we employed a capsule collider. Additionally, a slider-joint asset was used to represent the telescopic legs. The asset allows the user to set the telescoping length, spring constant, and damper constant. We used numerical simulations to optimize the elastic parameters of the robot (Fig. 6) shows the robot and its physical parameters, which we set according to Table 1. We set the Unity simulation parameters, listed in Table 2, to produce accurate a result while increasing the computational complexity.

3 Control method

We utilized input–output linearization and output-zeroing control to achieve the desired angle to control attitude of the torso. Despite the robot was 3D, the mathematical model for the control was defined as follows. 2D as the rimless wheel robot performed 2D motion while moving in the sagittal plane. If the leg extension/contraction is small, the robot's dynamics should be similar to a rimless wheel robot without

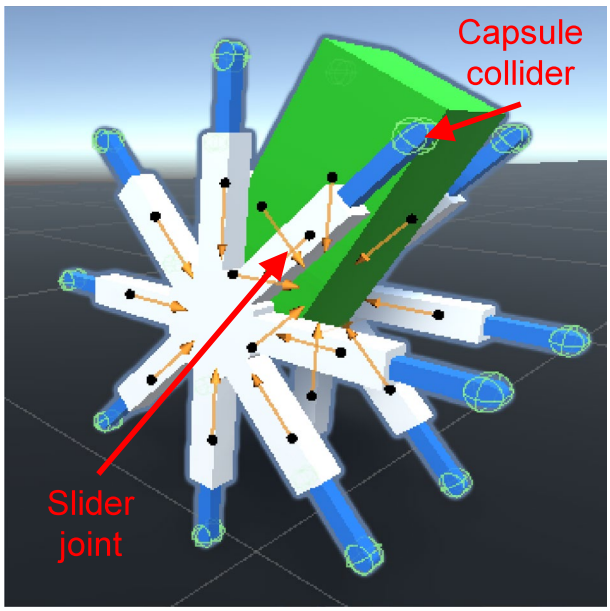

Fig. 5 Unity-based 3D model of the rimless wheel robot

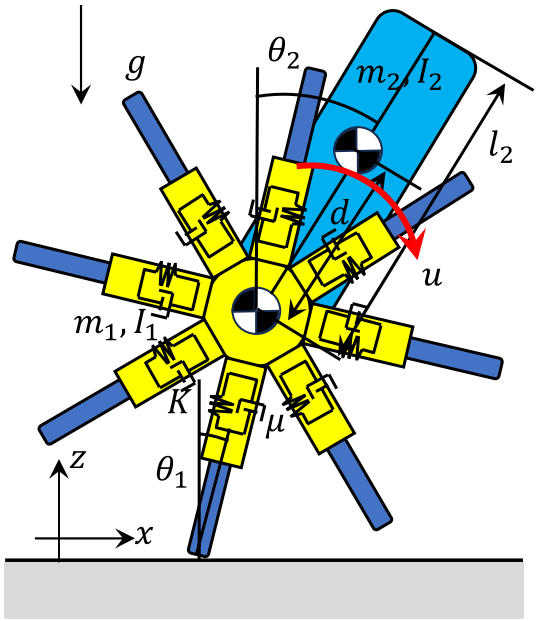

Fig. 6 Specified parameters of rimless wheel robot with elastic telescopic legs

Table 1 Physical parameters of the robot

Part	Symbol	Value	Unit
Mass of the wheel	m_1	0.651	kg
Mass of the torso	m_2	0.679	kg
Length of the legs	l_1	0.15	m
Length of the torso	l_2	0.182	m
CoG of the torso	d	0.095	m
Spring constant of the legs	K	–	N/m
Viscosity of the legs	μ	10	N · s/m
Moment of inertia of the wheel	I_{1xx}	0.006	kg · m^2
	I_{1xy}	3.535×10^{-5}	kg · m^2
	I_{1xz}	-1.362×10^{-5}	kg · m^2
	I_{1yy}	0.006	kg · m^2
	I_{1yz}	-3.085×10^{-5}	kg · m^2
	I_{1zz}	0.006	kg · m^2
Moment of inertia of the torso	I_{2xx}	0.003	kg · m^2
	I_{2xy}	-6.02×10^{-6}	kg · m^2
	I_{2xz}	6.825×10^{-7}	kg · m^2
	I_{2yy}	0.001	kg · m^2
	I_{2yz}	9.48×10^{-5}	kg · m^2
	I_{2zz}	0.003	kg · m^2

Table 2 Unity simulation parameters

Item	Value or setting
Dynamic and static friction	0.6 (Average)
Bounciness	0.4 (Average)
Bounce threshold	1.77
Default contact offset	0.2
Default solver iterations	25
Default solver velocity iterations	70
Friction type	two directional

leg extension/contraction. The following equation describes the motion of the rimless wheel robot without leg extension/contraction:

$$\boldsymbol{M}(\boldsymbol{q})\ddot{\boldsymbol{q}} + \boldsymbol{H}(\boldsymbol{q}, \dot{\boldsymbol{q}}) = \boldsymbol{S}u, \tag{1}$$

where $\boldsymbol{q} = [\theta_1,\ \theta_2]^{\mathrm{T}}$ is the generalized coordinate vector. Inertial matrix $\boldsymbol{M}(\boldsymbol{q}) \in \mathbb{R}^{2\times 2}$ is expressed as follows:

$$\boldsymbol{M}(\boldsymbol{q}) = \begin{bmatrix} I_{1zz} + (m_1 + m_2)l_1^2 & m_2 d l_1 \cos(\theta_1 - \theta_2) \\ m_2 d l_1 \cos(\theta_1 - \theta_2) & I_{2zz} + m_2 d^2 \end{bmatrix},$$

the Coriolis, centrifugal, and gravitational force vectors $\boldsymbol{H}(\boldsymbol{q}, \dot{\boldsymbol{q}}) \in \mathbb{R}^2$ is expressed as follows:

$$\boldsymbol{H}(\boldsymbol{q}, \dot{\boldsymbol{q}}) = \begin{bmatrix} m_2 d l_1 \sin(\theta_1 - \theta_2)\dot{\theta}_2^2 - (m_1 + m_2) l_1 g \sin\theta_1 \\ -m_2 d l_1 \sin(\theta_1 - \theta_2)\dot{\theta}_1^2 - m_2 d g \sin\theta_2 \end{bmatrix},$$

u is the input, and the driving matrix $\boldsymbol{S} \in \mathbb{R}^2$ is expressed as

$$\boldsymbol{S} = \begin{bmatrix} -1 \\ 1 \end{bmatrix}.$$

The equation for the affine system is defined as follows:

$$\begin{aligned} \frac{d}{dt}\begin{bmatrix} \boldsymbol{q} \\ \dot{\boldsymbol{q}} \end{bmatrix} &:= f_A(\boldsymbol{q}, \dot{\boldsymbol{q}}) + g_A(\boldsymbol{q})u. \\ f_A(\boldsymbol{q}, \dot{\boldsymbol{q}}) &= \begin{bmatrix} \dot{\boldsymbol{q}} \\ \boldsymbol{M}^{-1}(\boldsymbol{q})\,(-\boldsymbol{H}(\boldsymbol{q}, \dot{\boldsymbol{q}})) \end{bmatrix} \\ g_A(\boldsymbol{q}) &= \begin{bmatrix} 0 \\ \boldsymbol{M}^{-1}(\boldsymbol{q})\boldsymbol{S} \end{bmatrix} \end{aligned} \tag{2}$$

To converge the torso angle θ_2 to the desired value θ_{2d}, the output function is defined as follows:

$$y := h(q) = \theta_2 - \theta_{2d} = 0. \tag{3}$$

Differentiating this function with time yields the following functions [16].

Table 3 Control parameters of the robot

Name	Symbol	Value
Step size	dt	0.001 s
Desired torso angle	θ_{2d}	0.30 rad
Proportional gain	K_p	450
Differential gain	K_d	70
Gravitational acceleration	g	9.8

$$\begin{aligned} \frac{dy}{dt} &= \begin{bmatrix} \frac{\partial h}{\partial q} & 0 \end{bmatrix} \begin{bmatrix} \dot{\boldsymbol{q}} \\ \boldsymbol{M}^{-1}(\boldsymbol{q})\,(-\boldsymbol{H}(\boldsymbol{q}, \dot{\boldsymbol{q}})) \end{bmatrix} \\ &\quad + \begin{bmatrix} \frac{\partial h}{\partial q} & 0 \end{bmatrix} \begin{bmatrix} 0 \\ \boldsymbol{M}^{-1}(\boldsymbol{q})\boldsymbol{S} \end{bmatrix} u \\ &= L_f h + L_g h, \end{aligned} \tag{4}$$

$$\begin{aligned} \frac{d^2 y}{dt^2} &= \begin{bmatrix} \frac{\partial}{\partial q}\left(\frac{\partial h}{\partial q}\dot{q}\right) & \frac{\partial h}{\partial q} \end{bmatrix} \begin{bmatrix} \dot{\boldsymbol{q}} \\ \boldsymbol{M}^{-1}(\boldsymbol{q})\,(-\boldsymbol{H}(\boldsymbol{q}, \dot{\boldsymbol{q}})) \end{bmatrix} \\ &\quad + \frac{\partial h}{\partial q}\boldsymbol{M}^{-1}(\boldsymbol{q})\boldsymbol{S}u \\ &= L_f^2 h + L_g L_f h u. \end{aligned} \tag{5}$$

As the relative order of the system is two, the partially linearized feedback input for input–output linearization is given by

$$u = -\frac{1}{L_g L_f h}(L_f^2 h - v), \tag{6}$$

where $L_g L_f h$ and $L_f^2 h$ are provided by

$$\begin{aligned} L_g L_f h &= \boldsymbol{C}\boldsymbol{M}^{-1}(\boldsymbol{q})\boldsymbol{S}, \\ L_f^2 h &= -\boldsymbol{C}\boldsymbol{M}^{-1}(\boldsymbol{q})\boldsymbol{H}(\boldsymbol{q}, \dot{\boldsymbol{q}}), \\ \boldsymbol{C} &= \begin{bmatrix} 0 & 1 \end{bmatrix}. \end{aligned}$$

Finally, we set a new control input v as

$$v = -K_P(\theta_2 - \theta_{2d}) - K_d\dot{\theta}_2. \tag{7}$$

4 Walking analysis in unity

Figure 7 shows the walking environment of the rimless wheel. The robot model was placed in Unity space. Moreover, the floor and a step (the green object) were set. We first analyzed the walking speed and energy efficiency of the robot with respect to the spring constant of the legs on level ground. Table 3 presents the list of the control parameters of the robot. The initial condition of the robot was $\boldsymbol{x}_0 = [0.0, 0.30,\ 0.0,\ 0.0]^{\mathrm{T}}$, and the index of energy

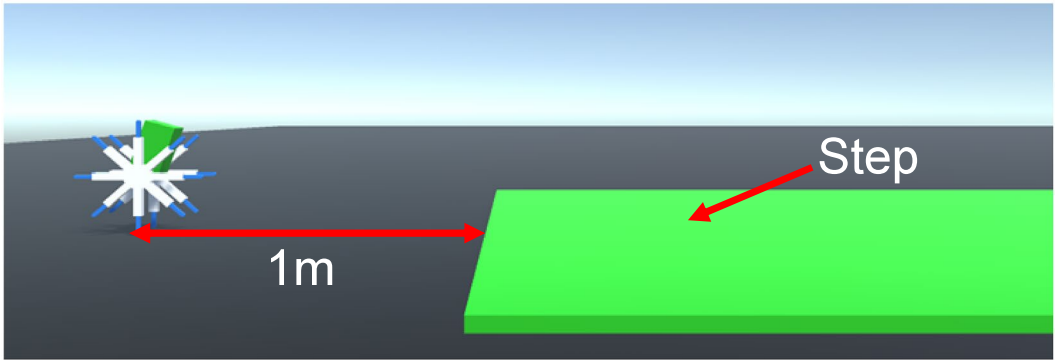

Fig. 7 Walking environment with a green object as a step

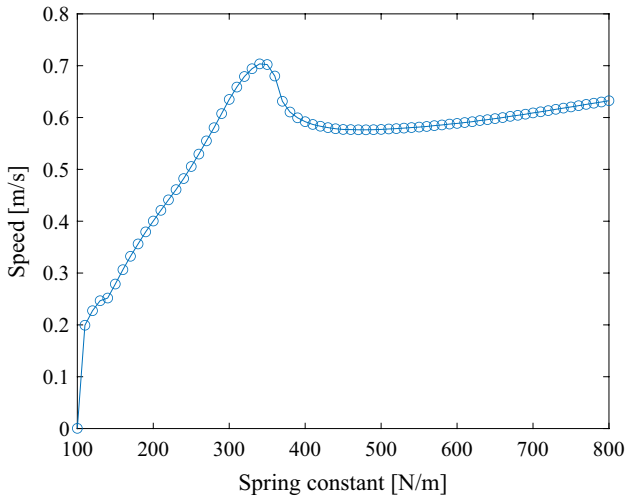

Fig. 8 Walking speeds on level ground with respect to the spring constant of the legs

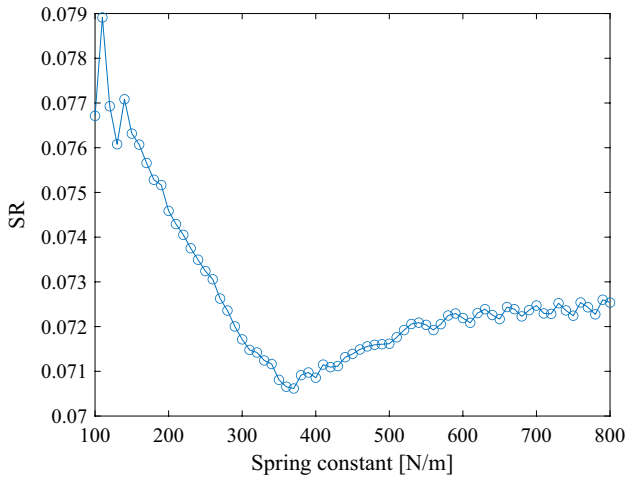

Fig. 9 Relation of Specific resistance on level ground with the spring constant of the legs

efficiency and specific resistance (SR) was calculated as follows:

$$\mathrm{SR} := \frac{p}{Mgv_a}, \tag{8}$$

where p [J/s] is the average input power, $M = m_1 + m_2$ [kg] is the total mass of the robot, and v_a is the average walking speed. The average input power of the robot is given by

$$p := \frac{1}{T}\int_0^T |u(\dot{\theta}_2 - \dot{\theta}_1)|\mathrm{d}t,$$

where T [s] is the total walking time.

Initially, Fig. 8 demonstrate the walking speed of the robot on level ground (i.e. no step case) with respect to the spring constant of the legs. The robot's walking speed depended on the spring constant, and it reached the maximum speed when the spring constant was 340 N/m. Figure 9 presents the variation in the SR of the robot while walking on level ground with respect to the spring constant of the legs. The spring constant is also correlated with SR. When the spring constant of the legs was 370 N/m, the robot walked most energy-efficiency with the lowest SR value.

Furthermore, we investigated the robot's ability to overcome different heights based on variation of the leg's spring constant. The ease of overcoming heights varied with the position between the legs and the step to be overcome. To divede stride length was into four parts, the following formula is employed: (i.e., $0.5 \times l_1 \times \sin(\pi/16)$) when the legs were not stretched or contracted, and the initial position before walking was categorized into four patterns. Then, when three of the four patterns overcame a step, it was defined as walking over a step. Figure 10 presents the heights of the steps overcome by the robot with respect to the spring constant of the legs. The spring constant affected the height of the steps that the robot could overcome, and there was a spring constant that

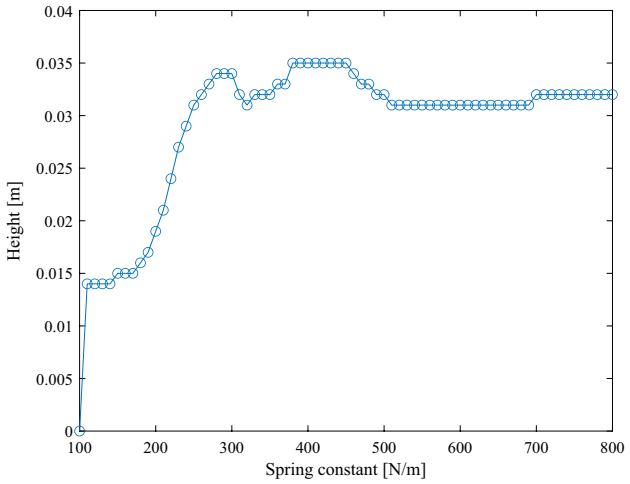

Fig. 10 Heights of steps overcome by the robot with respect to the spring constant of the legs

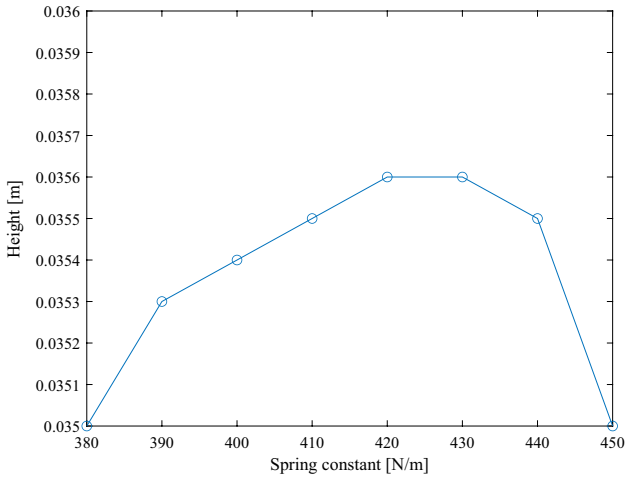

Fig. 11 More detailed analysis of the height of steps exceeded by the robot

enabled the robot to overcome the highest step. With the leg extension/retraction setting, the rimless wheel would overcome could overcome a 0.035 m high step. Figure 11 presents the results based on a more detailed examination of the steps between 380 and 450 N/m. The robot with spring constants 420 and 430 N/m overcame a step height of 0.0356 m.

Comparing level walking at 420 and 430 N/m in terms of walking speed (Fig. 8) and energy efficiency (Fig. 9), it was found that level walking at 420 N/m was superior in terms of walking speed and energy efficiency. Therefore, a spring constant of 420 N/m is optimum for the rimless wheel robot.

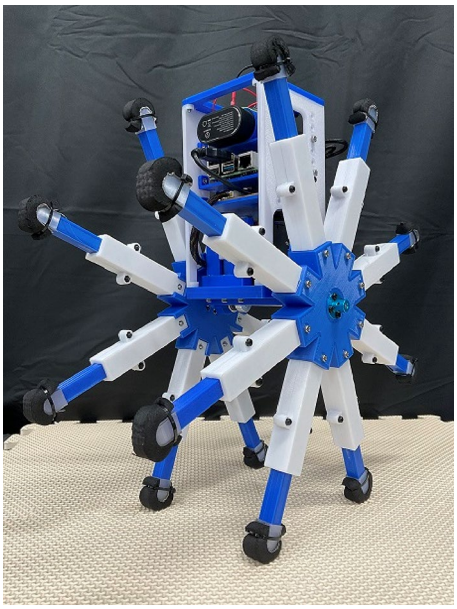

Fig. 12 Rimless wheel robot with elastic telescopic-legs

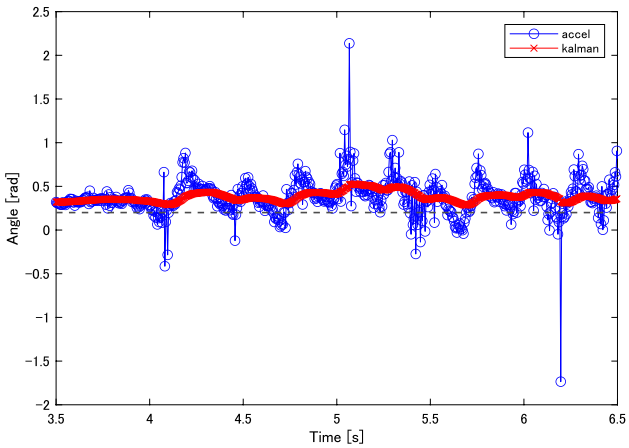

Fig. 13 Torso angle while walking on level ground

5 Walking experiments

First, we performed a walking experiment with the robot (Fig. 12) on level ground. However, as the developed robot cannot accurately gather the angle of the support legs, PD control was conducted using only the torso posture. Then, we made the experiment on the ground without and with a 0.03 m step (Approx. 20% of leg length). Figures 13 and 14 display the torso angles of the robot walking on level ground without and with a step, respectively. Comparing the two figures, the angle of the torso changed considerably during the period when the steps were overcome. Figures 15 and 16 present the sequential photos of walking on

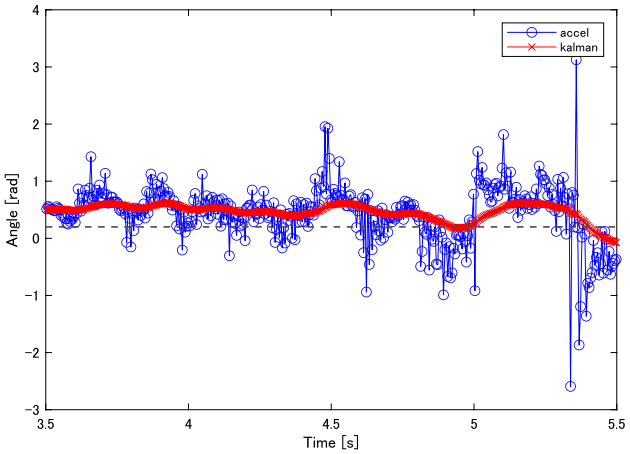

Fig. 14 Torso angle while walking on level ground with a step

level ground without and with a step, respectively. These figures demonstrate that the robot walked on level-ground and overcame the step.

6 Conclusion and future work

We simulated and analyzed the walking performance of a 3D model of a rimless-wheel robot with elastic telescopic legs in Unity. The leg's spring constant affected the robot's walking performance. The analyses revealed an optimum spring constant that enabled the robot to overcome the steps. Employing the optimal parameters, we constructed a rimless-wheel robot with elastic telescopic legs that could overcome steps. The robot could walk on level ground and surfaces with 0.03 m step. This rimless wheeled robot with leg elasticity optimization could cope passively with stepped environments and move at fast on stepped surfaces.

In the future, we will implement advanced control and optimize the robot's energy consumption during walking. We intend to develop a one-wheeled rimless wheeled robot so that the single-wheeled version can move in more confined spaces and consequently enhance the robot's versatility.

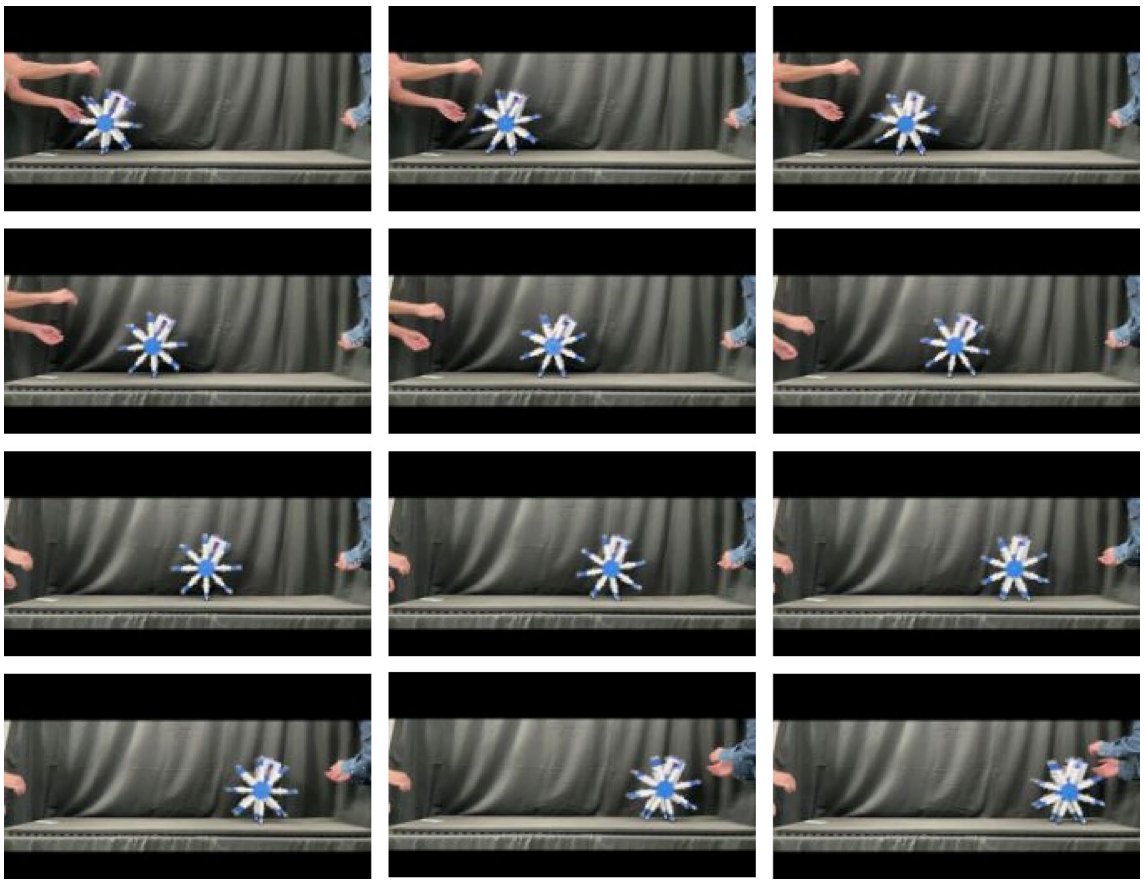

Fig. 15 Sequential photos of walking on level ground

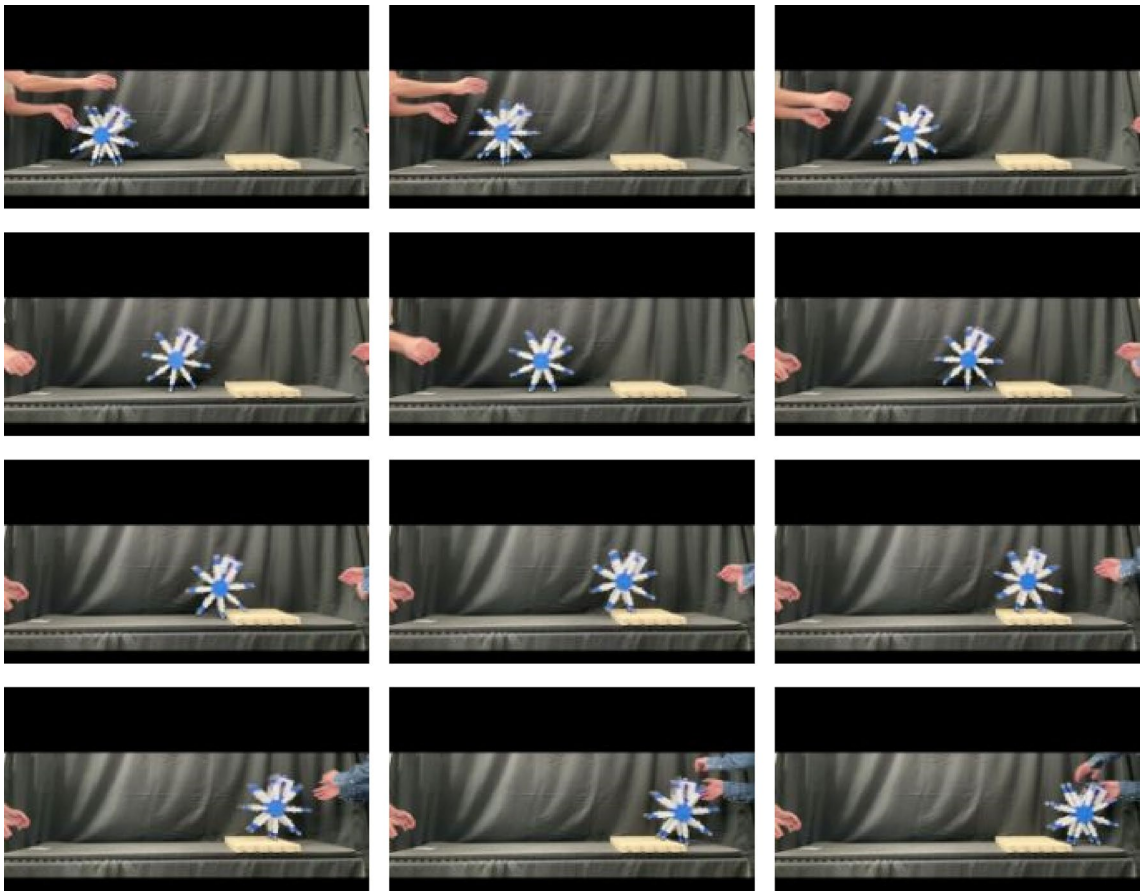

Fig. 16 Sequential photos of walking on level ground with a step

References

1. Mertyuz I, Tanyildizi AK, Tasar B, Tatar AB, Yakut O (2020) FUHAR: a transformable wheel-legged hybrid mobile robot. Robot Auton Syst 133:103627
2. Wei Z, Ping P, Luo Y, Liu J, Chen D, Wang W, Sun H, Song A, Song G (2024) A novel transformable leg-wheel mechanism. J Mech Robot 16(3):031008
3. McGeer T (1990) Passive dynamic walking. Int J Robot Res 9(2):62–82
4. Cleman MJ, Chatterjee A, Ruina A (1997) Motions of a rimless spoked wheel: a simple three-dimensional system with impacts. Dyn Stab Syst 12(3):139–159
5. Asano F, Luo ZW (2009) Asymptotically stable biped gait generation based on stability principle of rimless wheel. Robotica 27(6):949–958
6. Asano F, Suguro M (2012) Limit cycle walking, running, and skipping of telescopic-legged rimless wheel. Robotica 30(6):989–1003
7. Hanazawa Y (2018) Development of rimless wheel with controlled wobbling mass. In: Proceeding of IEEE/RSJ international conference on intelligent robots and systems (IROS), pp. 4333–4339
8. Hanazawa Y, Nishinami H, Sagara S (2022) Walking experiment of small and lightweight rimless wheel robot. J Artif Life Robot 27(4):706–713
9. Asano F, Kawamoto J (2012) Passive dynamic walking of viscoelastic-legged rimless wheel. In: Proceeding of IEEE/RSJ international conference on intelligent robots and systems (IROS), pp. 157–162
10. Kawamoto J, Asano F (2012) Active viscoelastic legged rimless wheel with upper body and its adaptability to irregular terrain.

In: Proceeding of IEEE/RSJ international conference on intelligent robots and systems (IROS), pp. 157–162
11. Asano F, Kawamoto J (2014) Modeling and analysis of passive viscoelastic-legged rimless wheel that generates measurable period of double-limb support. Multibody SysDyn 31:111–126
12. Jeans JB, Hong D (2009) IMPASS: Intelligent mobility platform with active spoke system. In: Proceeding of IEEE international conference on robotics and automation (ICRA), pp.1605-1606
13. hounsule PA, Ameperosa E, Miller S, Seay K, Ulep R (2016) Dead-beat control of walking for a torso-actuated rimless wheel using an event-based, discrete, linear controller. In: Proceeding of ASME international design engineering technical conferences and computers and information in engineering conference (IDETC/CIE), pp. 1-9
14. Sanchez S, Bhounsule PA (2021) Design, modeling, and control of a differential drive rimless wheel that can move straight and turn. Automation 2(3):98–115
15. Unity-Website "https://www.unity.com". (available)
16. Westervelt ER, Grizzle JW, Chevallereau C, Choi JH, Morris B (2018) Feedback control of dynamic bipedal robot locomotion. CRC Press, Taylor and Francis